

Last glacial cycle glacier erosion potential in the Alps

Julien Seguinot¹ and Ian Delaney²

¹Independent scholar, Anafi, Greece

²Institute of Earth Surface Dynamics, University of Lausanne, Switzerland

Abstract.

The glacial landscape of the Alps has fascinated generations of explorers, artists, mountaineers and scientists with its diversity, including erosional features of all scales from high-mountain cirques, to steep glacial valleys and large over-deepened basins. Using previous glacier modelling results, and empirical inferences of bedrock erosion under modern glaciers, we compute a distribution of potential glacier erosion in the Alps over the last glacial cycle from 120 000 years ago to the present. Despite large uncertainties pertaining to the climate history of the Alps and unconstrained glacier erosion processes, the resulting modelled patterns of glacier erosion include persistent features. The cumulative imprint of the last glacial cycle shows a very strong localization of erosion potential with local maxima at the mouths of major Alpine valleys and some other upstream sections where glaciers are modelled to have flown with the highest velocity. The potential erosion rates vary significantly through the glacial cycle, but show paradoxically little relation to the total glacier volume. Phases of glacier advance and maximum extension see a localization of rapid potential erosion rates at low elevation, while glacier erosion at higher elevation is modelled to date from phases of less extensive glaciation. The modelled erosion rates peak during deglaciation phases, when frontal retreat results in steeper glacier surface slopes, implying that climatic conditions that result in rapid glacier erosion might be quite transient and specific. Our results depict the Alpine glacier erosion landscape as a time-transgressive patchwork, with different parts of the range corresponding to different glaciation stages and time periods.

1 Introduction

The glacial erosion landscape of the Alps has fascinated generations of explorers, artists, mountaineers and scientists for centuries. Its cultural impact is indeed so far-reaching, that in English, a non-Alpine language, the adjective “alpine” with non-capital “a” is now casually used to describe an Alpine-like, glacially modified mountain landscape outside the Alps, while the proper noun “Alps” has been applied to nick-name Alpine-like, glacier eroded mountain ranges in Norway (*Lyngsalpene*), New Zealand (Southern Alps), Japan (日本アルプス, *Nihon Arupusu*), and elsewhere. Some mountain ranges are predominantly characterised by cirque glaciation (e.g. Uinta Mountains), glacial valleys (e.g. Putorana Plateau), or large-scale overdeepenings (e.g. Patagonia). But other regions, including the Alps (e.g. Penck, 1905), present a higher variety of glacier erosional landforms, whose implications on glacial history are yet to be understood. In parallel to such landscape diversity, the cosmogenic nuclide memory of bedrock erosion provides a more quantitative, but equally varied picture of glacier erosion effectiveness both within and between glaciated regions (Jansen et al., 2019; Steinemann et al., 2020, 2021).

Glacially eroded topography has sometimes been used as a proxy for mapping paleoglacier extent (e.g., Margold et al., 2011; Fu et al., 2012). Cold-based glaciers, however, have been observed to preserve landforms as fragile as sand beaches (Kleman, 1994), leading to the reinterpretation of complex glacial landscapes within a binary conceptual framework of cold and temperate basal thermal regimes (Kleman et al., 2008, 2010; Fabel et al., 2012; Fu et al., 2013). Nevertheless, it remains elusive whether glacial topography is a proxy for temperate ice-cover duration, and why some glaciated regions show preserved periglacial blockfields topped by erratic boulders and others, including the Alps, do not (Wirsig et al., 2016; Seguinot et al., 2018).

On a larger scale, glacier erosion also likely governs, at least in part, the height of mountains (Egholm et al., 2009; Thomson et al., 2010) through the “glacier buzz-saw”. In turn, evidence suggests that increased mountain erosion rates coincided with global cooling and Pleistocene glaciations from roughly 2.6 million years before present (Herman and Champagnac, 2016). However, oceanic isotopic proxies for global weathering rates remained constant over this time period (Willenbring and Von Blanckenburg, 2010). Examination of contemporary erosion rates across different climates suggests that increased temperatures within glaciated regions lead to higher erosion rates (Koppes and Montgomery, 2009; Koppes et al., 2015; Fernandez et al., 2016). However, understanding the link between climate and glacier erosion in the sedimentary record remains difficult due to time scale biases (Ganti et al., 2016) and the non-linear relationship between atmospheric temperature and erosion (e.g., Anderson et al., 2012; Mariotti et al., 2021). Numerical glacier modelling may provide insights into such complexity.

Observing and quantifying the long-term glacier erosion and sedimentation processes has been a challenge, and two general methods have been adopted to quantify erosion (Alley et al., 2019). Physically-based models describe quarrying process and abrasion of bedrock by debris-laden ice (e.g., Alley et al., 1997; Iverson, 2012; Beaud et al., 2014). Describing the processes physically provides a basis for understanding erosion processes (Hallet, 1979; Ugelvig et al., 2018) and yields insight into the formation of glacial landforms, such as tunnel valleys and eskers (Beaud et al., 2018; Hewitt and Creyts, 2019). Yet, these models prove difficult to implement in many cases due to the large number of poorly constrained parameters and processes, i.e. water pressure fluctuations and subglacial debris concentration (e.g., Hallet, 1979; Seguinot, 2008; Ugelvig et al., 2018).

Instead, empirical relationships between glacier sliding and erosion can represent erosional quantities well and can recreate important glacial landforms (e.g., Harbor et al., 1988; MacGregor et al., 2000). For instance, Humphrey and Raymond (1994) correlated temporal variations in ice velocity and suspended sediment load during a surge of Variegated Glacier to establish a linear erosion law. Koppes et al. (2015) quantified sediment yields in 15 Patagonian and Antarctic Peninsula fjords, concluding at a predominant control of surface air temperature on rapid glacier erosion and calibrating a near-square-law from glacier velocity to erosion rate. Herman et al. (2015) collected suspended sediment samples for 5 months in the outlet stream of Franz-Josef Glacier, mapped their chemical composition to geologic zones of distinctive glacier speed, and also concluded to a near-square relationship between basal sliding and glacier erosion. Cook et al. (2020) assembled a global compilation of erosion rates for 38 glaciers, showing a predominant role of glacier sliding velocity over climate variables, yet concluding at a sub-linear relationship to erosion.

Here, the non-linear erosion law by Koppes et al. (2015) is applied to previously published model results (Seguinot et al., 2018) and the patterns of modelled erosion potential and cumulative last glacial cycle erosion potential are analysed. We

examine the glaciological conditions that cause erosion and discuss the implications of these conditions on understanding the mark of ancient glaciers on Alpine topography and the relationship between climate and glacier erosion. Despite aggregated uncertainties on paleoclimate, glacier flow and glacier erosion processes, our results provide insights into the diversity of the
65 Alpine glacial erosion landscape.

2 Methods

2.1 Ice sheet modelling

The ice-sheet model set-up was presented in an earlier publication (Seguinot et al., 2018) and is briefly summarized here. The simulations were conducted using the Parallel Ice Sheet Model (PISM, development version e9d2d1f), an open-source,
70 finite-difference, shallow-ice and shallow-shelf model (the PISM authors, 2017). Our setup includes temperature and water-content dependent creep, pseudo-plastic basal sliding, bedrock isostatic deformation under the ice load, and a positive degree-day (PDD) surface mass balance model. The model is initialized with assumed present-day ice thickness and 1-km resolution bedrock topography from SRTM (Jarvis et al., 2008), ice and bedrock temperature at 120 ka (thousand years before the present), and is run to the present. The ice-sheet model physical parameters are listed in the earlier open-access publication (Seguinot
75 et al., 2018), and the complete list of PISM parameters is stored in long-term archived model output metadata for the present study (Seguinot, 2021), and for the earlier publication (Seguinot, 2020a, b).

Climate forcing is provided by a monthly climatology from interpolated observational data (WorldClim; Hijmans et al., 2005) and the European Centre for Medium-Range Weather Forecasts Reanalysis Interim (ERA-Interim; Dee et al., 2011), amended with temperature changes from the European Project for Ice Coring in Antarctica (EPICA; Jouzel et al., 2007),
80 and time-dependent paleo-precipitation reductions (Huybrechts, 2002). Coarser, 2-km resolution runs based on alternative paleoclimate scenarios (Seguinot et al., 2018), forced by temperature changes from the the Greenland Ice Core Project (GRIP; Dansgaard et al., 1993) and an oceanic sediment core from the Iberian margin (MD01-2444; Martrat et al., 2007), are analyzed in the discussion part (Sect. 4.1).

2.2 Erosion law

85 Modelled erosion rates, \dot{e} , are calculated from the modelled basal velocities, u_b , using an empirical erosion power-law,

$$\dot{e} = K_g u_b^l, \tag{1}$$

where $K_g = 5.2 \times 10^{-11} \text{ m}^{1-l} \text{ a}^{l-1}$ and $l = 2.34$ are empirical constants calibrated on quantified fjord sediment yields and velocities from 15 Patagonian and Antarctic Peninsula tidewater glaciers (using the full dataset from Koppes et al., 2015, including outliers). We discuss the role of alternative values of K_g and l in the discussion part (Sect. 4.2).

90 Our approach does not account for feedbacks of glacier erosion onto bedrock topography and, then onto, ice dynamics (e.g., Anderson et al., 2012). Furthermore, we do not account for the downstream advection of debris (e.g., Anderson and Anderson, 2016), or fluvial transport of subglacial sediment (Delaney et al., 2019). Instead, we assume that eroded material is instantly

transported out of the system, thus neglecting its role in shielding the bedrock from glacier erosion in zones of temporary storage (Preusser et al., 2010). Neither do we account for differences in erosion effectiveness on different lithologies or erosion from subglacial and interglacial hydrologic processes. For the aforementioned reasons, we refer to the above computed rates, \dot{e} , as “potential erosion rates”.

Secondly, we compute the time-integrated glacier erosion rate,

$$e = K_g \int u_b^l dt, \quad (2)$$

and refer to it as the “cumulative erosion potential”. The integration is numerically approximated using a time-step of 10 a in the main simulation, and 100 a in the alternative climate scenarios runs. Note that in the above formula with an exponent, l , higher than one, the cumulative erosion potential has a greater dependency on the basal ice dynamics, u_b , than the duration of glacier cover.

3 Results

3.1 Cumulative erosion

The modelled cumulative (time-integrated) glacial erosion potential (Fig. 1a) varies by several orders of magnitude from insignificant to hundred-metres-scale erosion potential. Its spatial patterns show a very strong localization along the Alpine valleys, with local maxima occurring both at the Alpine gates where ice flow transited from valley to piedmont glaciers, and further upstream where the valley slopes increase. While mountain cirque glaciers and relevant erosion processes may not be captured by the model physics and horizontal resolution, high cumulative erosion potential also occurs near the valley heads. There is a general tendency for higher cumulative erosion in the north-western Alps where the input winter precipitation is higher (WorldClim, Fig. 1h in Seguinot et al., 2018) and the glacial relief more pronounced in the topography.

3.2 Temporal evolution

The modelled annual (domain-integrated) potential glacial erosion volume does not systematically correlate with the modelled total ice volume (Fig. 1b). Except for the onset and termination of the glacial cycle where ice volume is low and sliding processes unlikely to be captured by the model resolution, a comparison between the modelled ice volume and the modelled annual erosion volume shows no single relation between these two quantities (Fig. 2). After significant ice volume has been reached, there is a general tendency for slower erosion during periods of extensive glaciation (Fig. 2). However, the domain-integrated erosion volume is modelled to be consistently higher (by a factor 2 to 10) during periods of decreasing ice volume, than during periods of increasing ice volume (Fig. 2).

3.3 Spatial migration

A closer look at the Rhine Glacier, one of the paleo-ice sheet’s largest outlets, reveals a spatial migration of the modelled rapid erosion areas. During stages of glacier advance and maximum extension, erosion is modelled to be under 1 mm a^{-1} and

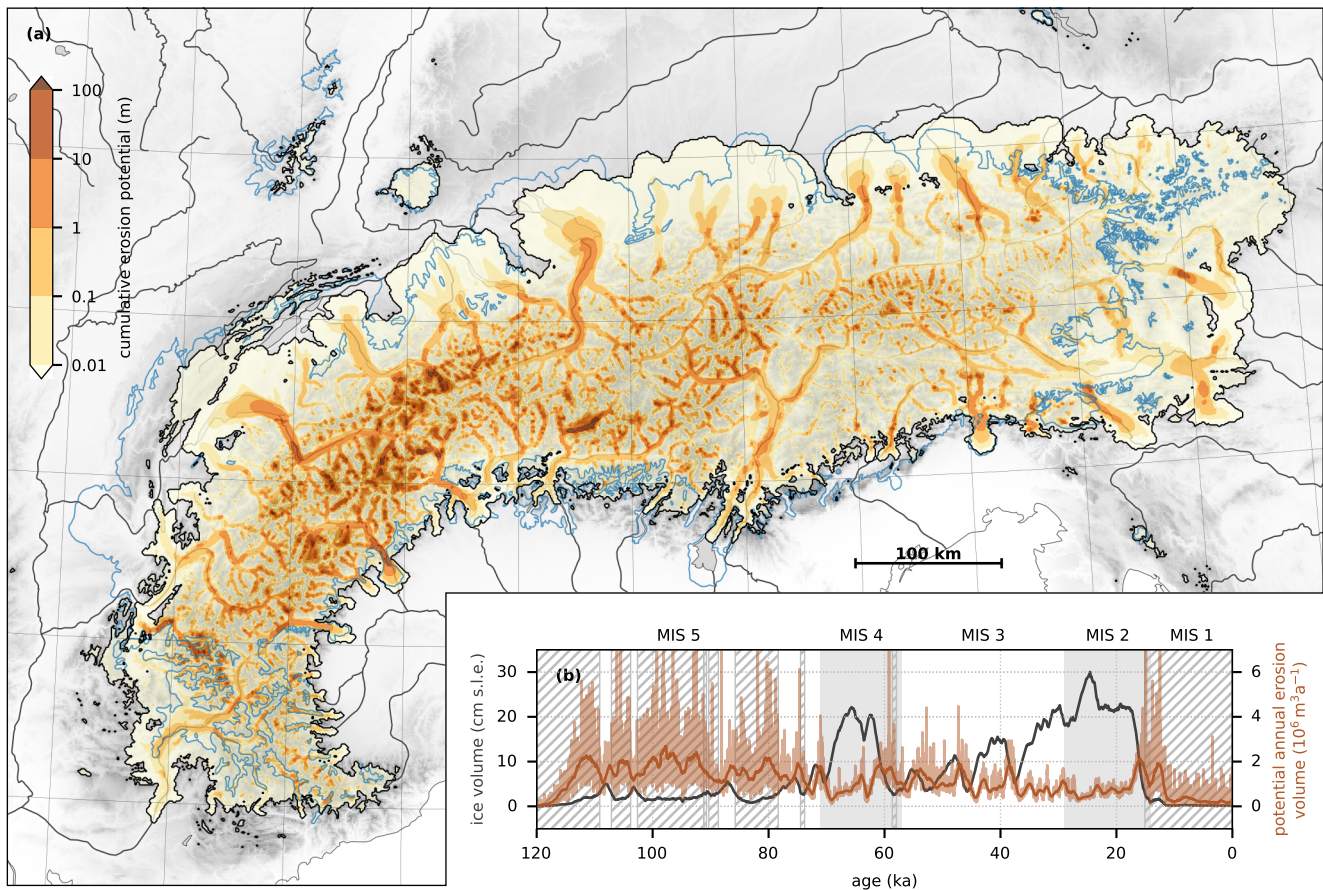


Figure 1. (a) Modelled cumulative (time-integrated) glacial erosion potential over the last glacial cycle and geomorphological reconstruction of Last Glacial Maximum Alpine glacier extent for comparison (solid blue line, Ehlers et al., 2011). The background maps consists of the initial basal topography from SRTM (Jarvis et al., 2008) and Natural Earth Data (Patterson and Kelso, 2017). (b) Modelled total ice volume in centimetres of sea-level equivalent (cm s.l.e., black), annual (domain-integrated) potential erosion volume (light brown) and its 1-ka running mean (dark brown). Shaded gray areas indicate the timing for MIS 2 and 4 (Lisiecki and Raymo, 2005). Hatches mark periods with ice volume below 3 cm s.l.e. where glacier sliding may be affected by stress-balance approximations and model horizontal resolution (see Sect. 4.4).

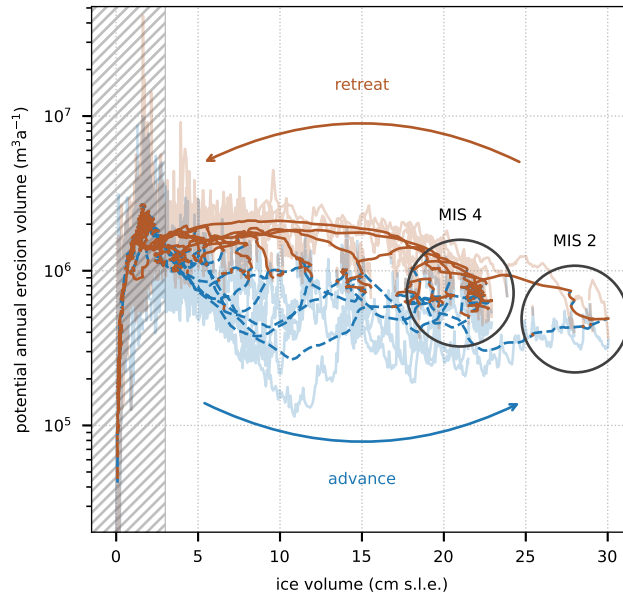


Figure 2. Modelled annual (domain-integrated) potential erosion volume (light curves) and its 1-ka running mean (dark curves) in relation to the modelled total ice volume in centimetres of sea-level equivalent. Blue dashes indicates increasing ice volume and solid brown decreasing ice volume. Hatches indicate low confidence due to limited glacier volume.

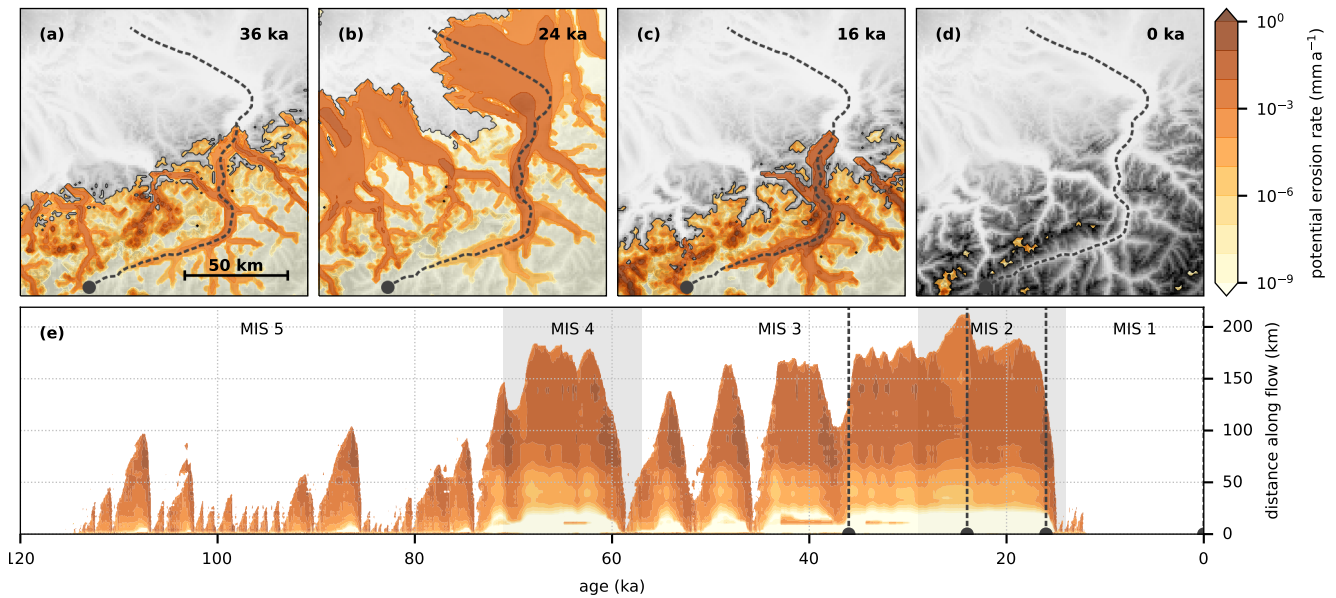


Figure 3. (a–d) Modelled instantaneous potential erosion rate of the Rhine Glacier for selected glacier advance and retreat ages, and the final model state for topographic reference. (e) Interpolated instantaneous potential erosion rate along a Rhine Glacier transect (upper panels dashed line) for the entire last glacial cycle.

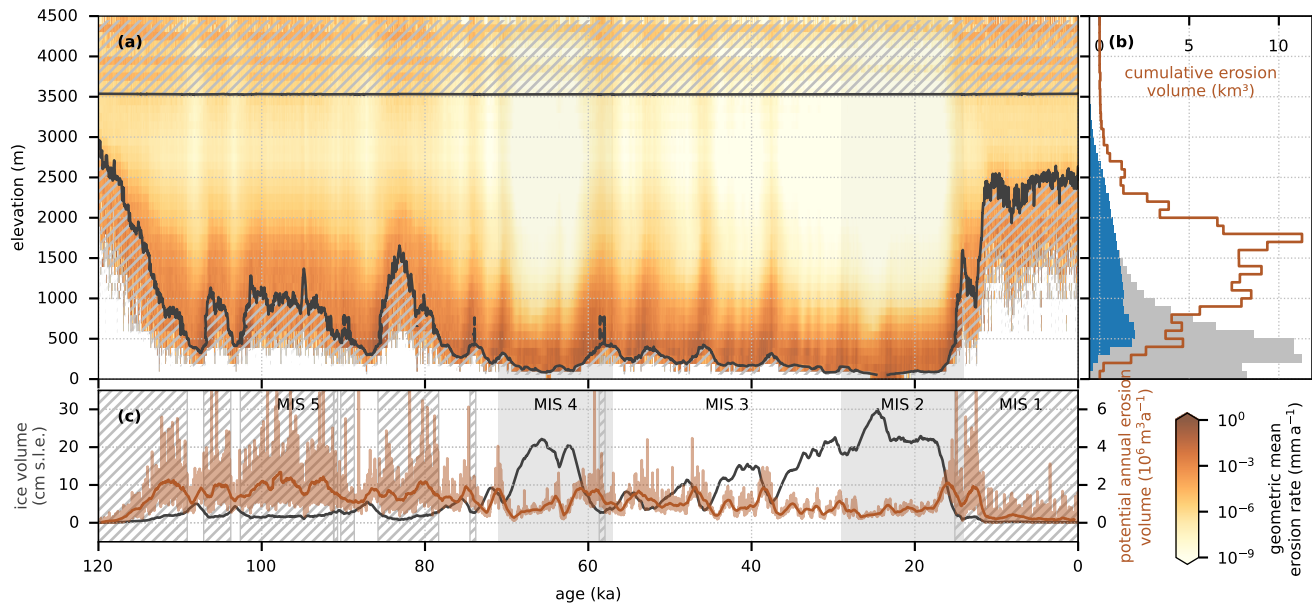


Figure 4. (a) Potential erosion rate “hypsogram”, showing the geometric mean of modelled rates in 100-m elevation bands across the entire model domain and its time evolution. Hatches indicate elevation bands with fewer than a hundred grid cells (100 km^2). (b) Distribution of model domain bedrock topography (grey bars) and glaciated topography (blue bars) in 100-m elevation bands, and the corresponding cumulative potential erosion volume (brown line). (c) Same as Fig. 1b.

restricted the lower parts of the catchment, while much of the intra-montane Alps (modelled to be largely cold-based, Fig. 6c in Seguinot et al., 2018) experience insignificant erosion potential (Fig. 3a and b). The potential erosion rates both increase and propagate inwards during periods of glacier retreat (Fig. 3c and e).

The results found on the Rhine Glacier catchment can be generalized to the entire model domain by using (present-day) bedrock altitude as a proxy for along-flow distance (Fig. 4). Thus more generally, periods of modelled increasing and maximum ice volume correspond to lower values for elevation-aggregated potential erosion rates, with significant erosion potential restricted to lower elevations. On the opposite, periods of modelled decreased ice volume correspond to higher local modelled erosion rates and more extensive rapid erosion potential into higher-elevation areas (Fig. 4).

4 Discussion

4.1 Climate sensitivity

Different paleoclimate forcing scenarios lead to different modelled glaciation histories (cf. Seguinot et al., 2018) and thus different results in terms of glacial cycle cumulative erosion potential (Fig. 5). Scenarios including higher (constant, present-day) input precipitation rates yield generally higher modelled ice discharge and thus higher erosion potential (Fig. 5a–c), while

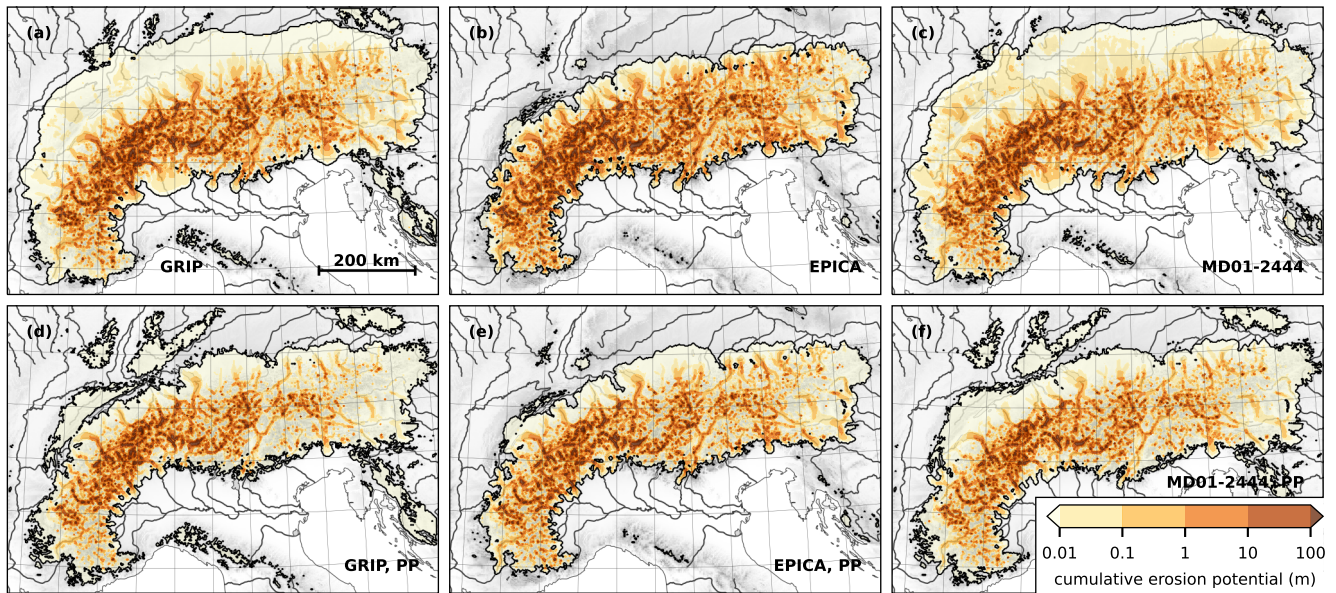


Figure 5. Modelled cumulative glacial erosion potential over the last glacial cycle using three different paleo-temperature histories from (a, d) the Greenland Ice Core Project (GRIP; Dansgaard et al., 1993), (b, e) the European Project for Ice Coring in Antarctica (our default, EPICA; Jouzel et al., 2007), and (c, f) an oceanic sediment core from the Iberian margin (MD01-2444; Martrat et al., 2007), and both (a–c) without and (d–f) with paleo-precipitation reductions (cf. Seguinot et al., 2018).

scenarios including paleo-precipitation reductions (Fig. 5d–f), including our default high-resolution run (Fig. 1), yield a smaller erosion potential.

The spatial pattern of modelled time-integrated erosion is nevertheless generally consistent across the paleoclimate scenarios tested, despite variations in the glaciation maximum extent (Fig. 3 in Seguinot et al., 2018; Fig. 5). It should be noted, however, that all runs presented here show a systematic bias with excessive glacier cover in the Eastern Alps and a diminished glacier extent in the Western Alps (Fig. 1a; further discussed in Seguinot et al., 2018). Thus the modelled patterns of erosion potential certainly includes a similar bias. However, uncertainties due to paleoclimate appear minor in regard to the much larger uncertainties affecting the choice of erosion law.

4.2 Choice of erosion law

The choice of erosion law significantly impacts the results (Fig. 6). Our default, based on quantified sediment yields from Patagonian and Antarctic Peninsula tidewater glaciers ($\dot{\epsilon} = 5.2 \times 10^{-8} u_b^{2.34}$, Koppes et al., 2015) yields a moderate and strongly localized cumulative erosion potential (Figs 1 and 6a). The erosion law based on measured suspended sediment load from Franz-Joseph Glacier ($\dot{\epsilon} = 2.7 \times 10^{-7} u_b^{2.02}$, Herman et al., 2015) also yields a strongly localized, and yet much higher, modelled erosion potential (Fig. 6b). The erosion law based on measured suspended sediment load during a surge of Variegated

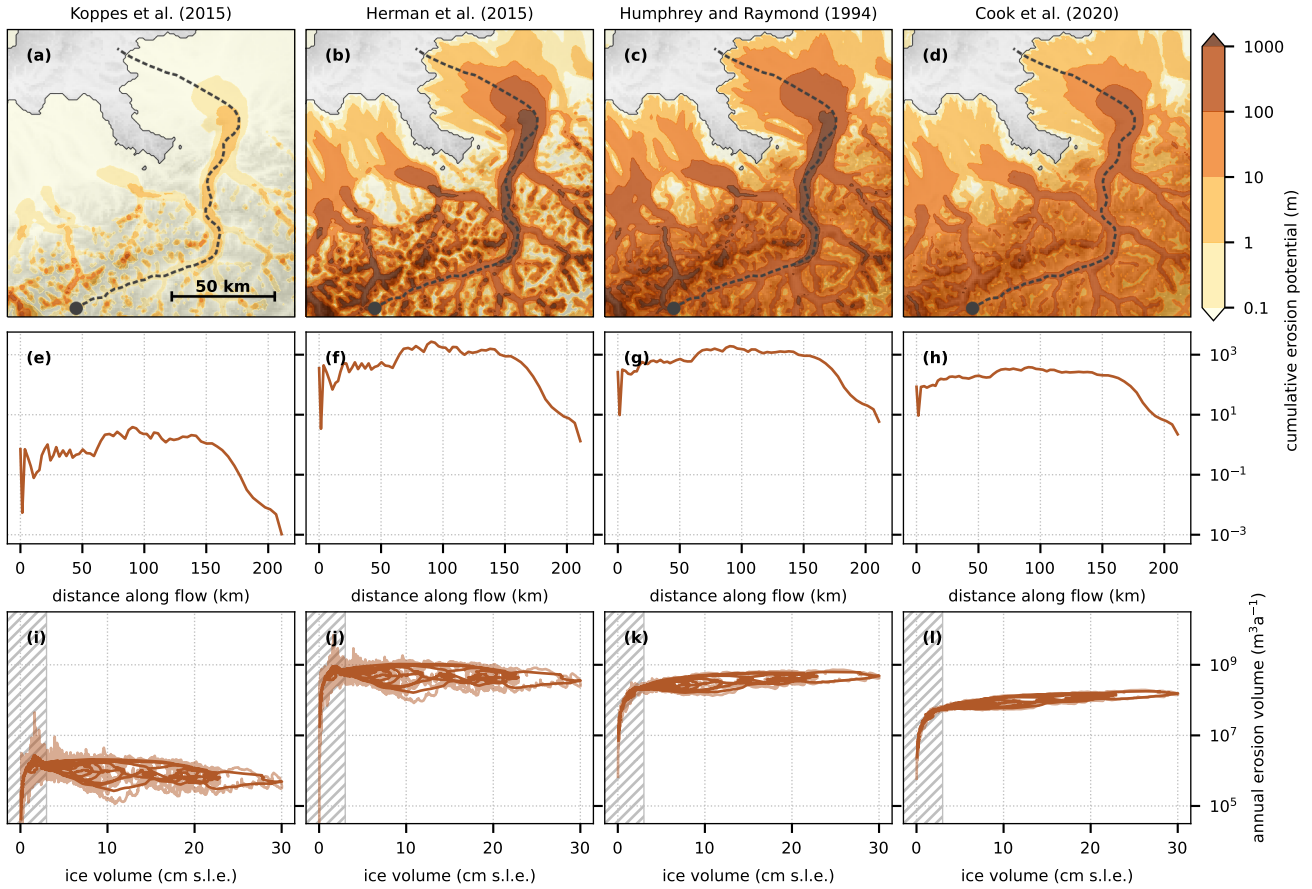


Figure 6. Modelled cumulative (time-integrated) glacial erosion potential for three different erosion laws published by (a) Koppes et al. (2015), $5.2 \times 10^{-8} u_b^{2.34}$ (same as Fig. 1a but with a different colour scale), (b) Herman et al. (2015), $2.7 \times 10^{-7} u_b^{2.02}$, (c) Humphrey and Raymond (1994), $1 \times 10^{-4} u_b^1$, and (d) Cook et al. (2020), $1.665 \times 10^{-1} u_b^{0.6459}$. (e-h) Corresponding modelled cumulative glacial erosion potential along a Rhine Glacier transect (upper panels dashed line), and (i-l) corresponding modelled evolution of annual (domain-integrated) erosion volume (light brown) and 1-ka running mean (dark brown) in relation to modelled total ice volume in centimetres of sea-level equivalent (as in Fig. 2a).

150 Glacier ($\dot{\epsilon} = 1 \times 10^{-4} u_b^1$, Humphrey and Raymond, 1994) results in similarly high values, but a less localized pattern of cumulative erosion potential (Fig. 6c). Finally, The erosion law based on a global compilation of glacier velocities and erosion rates ($\dot{\epsilon} = 1.665 \times 10^{-1} u_b^{0.6459}$, Cook et al., 2020) yields an even flatter pattern of cumulative erosion potential (Fig. 6d).

With a total Pleistocene glacial relief on the order of a kilometre (Preusser et al., 2011; Valla et al., 2011), a cumulative glacial erosion for the last glacial cycle in the order of 10 to 100 m can be expected. However, none of the tested erosion power-laws
 155 fall within this range. Instead, the erosion law calibrated on tidewater glaciers (Koppes et al., 2015) yields cumulative erosion in the Rhine Valley in the orders of metres, while the three erosion laws based on terrestrial glaciers (Humphrey and Raymond,

1994; Herman et al., 2015; Cook et al., 2020), result in kilometre-scale integrated erosion potential. During the Last Glacial Maximum and much of the last glacial cycle, Alpine paleoglaciers were closer in size, slope (an important parameter as we argue in the next section), and climatic context to the present-day glaciers of Patagonia and the Antarctic Peninsula (Koppes et al., 2015) than to Franz-Joseph Glacier (Herman et al., 2015) and many of the glaciers included in the global compilation by Cook et al. (2020). This may help to explain why the reality appears to fall in-between the tested erosion laws.

That said, the magnitude of the modelled erosion rates can hardly be used as a criteria to rule out this or that erosion law for the glacial Alps. While sliding is here modelled by a pseudo-plastic law based on till dilatation under high water pressure (Tulaczyk et al., 2000), empirical erosion rules are thought to be a proxy for glacier abrasion (cf. Hallet, 1979; and possibly plucking) of a glacier flowing over a hard bed. Current erosion rates in the Alps strongly vary depending on the substratum (Steinemann et al., 2020, 2021), and it is arguable that a layer of till and proglacial sediments may have armored the glacier bed from erosion for at least parts of the glacial cycle. Thus, given the lack of data to constrain the erosion rule, it can not be excluded that a linear or sub-linear erosion law (e.g., Cook et al., 2020) would lead to a less localized pattern of erosion (Fig. 6c and d), and a stronger correlation between modelled ice volume and erosion (Fig. 6k and l). On the other extreme, an even more non-linear erosion law, not tested here, derived from tidewater glaciers but excluding two outliers ($\dot{e} = 5.3 \times 10^{-9} u_b^{2.62}$, Koppes et al., 2015) would result in an even more localized pattern of erosion potential.

The modelled pattern of erosion potential depends on PISM glacier physics and sliding model parameters. In particular, the pseudo-plastic sliding law exponent ($q = 0.25$ in Seguinot et al., 2018) controls the sharpness of the transition between adherent and decoupled basal conditions. Recent ensemble validation of Antarctic Ice Sheet glacial-cycle simulations against geological and present-day observations (Albrecht et al., 2020a, b) support a higher value of $q = 0.75$, and thus a sliding law closer to linear, which would perhaps result in a smoother distribution of sliding velocity and erosion potential. Lateral stress gradients missing from the shallow-shelf approximation stress balance could also contribute to moderate sliding velocity in narrow troughs (Herman et al., 2011; Egholm et al., 2012a, b; Pedersen et al., 2014).

Because of the intrinsically large variations in modelled glacier sliding velocities yield cumulative glacial-cycle erosion two to three orders of magnitude higher in the Alpine valleys than near the mountain tops (Fig. 6d), we argue that the modelled highly localized pattern of erosion potential is qualitatively robust. This pattern, and the lithologic variations in bedrock erodability, may explain order-of-magnitude variation of glacier erosion rates observed in the cosmogenic nuclide record (Jansen et al., 2019; Steinemann et al., 2020, 2021).

4.3 Climate control on erosion

The modelled, domain-integrated glacier erosion volume does not increase together with ice volume. On the opposite, periods of ice advance and maximum glaciation correspond to comparatively slow erosion potential (Figs. 1 and 2). This result may seem paradoxical, and is modulated in a limited extent by the exponent, l , in the erosion rule (Fig. 6). Nevertheless, it may explain why some areas covered during glacial maxima only, such as some valleys on the southern side of the Alps, appear to have experienced only little glacial modification of their topography. During deglaciation periods, increased surface melt at low elevations results in a steepened topographic profile (Figs. 7a), as observed and further expected on currently retreating

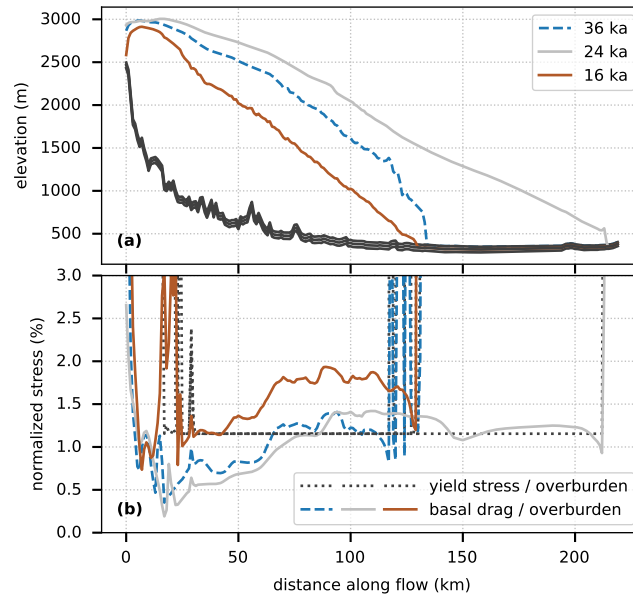


Figure 7. (a) Modelled basal and surface topographies interpolated along the Rhine Glacier during glacier advance (36 ka, dashed blue), maximum extent (24 ka, solid grey) and retreat (16 ka, solid brown, using the same transect as in Fig. 7). **(b)** Interpolated yield stress in the pseudo-plastic sliding law (dotted lines) and magnitude of the basal shear stress (basal drag, solid lines), both normalized against the ice overburden pressure. Basal drag values greater than yield stress result in glacier sliding (cf. Seguinot, 2014; Seguinot et al., 2016, for model physics). Some of the observed basal drag fluctuations in the upper part of the transect result from steep slopes on either side of the narrow valley.

glaciers (Huss et al., 2010; Zekollari and Huybrechts, 2015). The buttress formed by the glacier foot against gravitational forces is reduced, causing an increase in the magnitude of the basal shear stress (basal drag) relative to the ice overburden pressure, and an increase in the area where sliding and thus, erosion, can occur (Figs. 7b).

This result is corroborated by a recent denudation record from the Mediterranean Alps, which includes an increase in glacier erosion in the Var Valley, roughly at 25 ka following an extended period of low denudation rates (Mariotti et al., 2021). While that increase in erosion predates the increase observed in our study (ca. 15 ka; Fig. 2), it demonstrates that climatic conditions over which glacier erosion occurs are relatively specific and likely transient. Other field-based studies have evidenced increased glacier erosion and pro-glacial sedimentation during the current deglaciation period (e.g., Koppes and Montgomery, 2009; Micheletti and Lane, 2016; Lane et al., 2017; Bendixen et al., 2017). This increase has often been attributed to higher meltwater availability, promoting sediment transport (Delaney and Adhikari, 2020), enhanced glacier sliding (Herman et al., 2011), and hydrofracturing, i.e. plucking (Hallet, 1996; Ugelvig et al., 2018; Hildes et al., 2004).

But importantly, these hydrological processes are not included in our model, so that deglaciation surface meltwater is assumed to instantly exit the glacier with no effect on glacier dynamics (cf. Werder et al., 2013; Iverson, 2012; Ugelvig et al., 2018, for comparison). The enhanced glacier velocity during periods of ice retreat is here modelled to result from changes in



Figure 8. Alpine glacial erosion landscape diversity. (a) Piedmont overdeepening of Lake Constance, ca. 10x50 km. (b) Glacial trough at Bout du Monde, ca. 1x10 km. (c) The unusually deep mountain cirque revealed by the current demise of Chüebodengletscher, ca. 1x1 km.

205 glacier geometry alone (Figs. 7b). Coincidentally, the link between climate and erosion is also the topic of a recent, independent study using PISM (Lai and Anders, 2021). Observed feedbacks between surface meltwater and basal sliding, not included in the model, presumably further accelerated erosion during deglaciation (Herman et al., 2011). Furthermore, we omit the fluvial transport of sediment, which could well increase sediment discharge and erosion with increased melt, so long as additional sediment remains available (Delaney and Adhikari, 2020). Rapid glacier erosion can be expected to accompany the ongoing
 210 21st-century deglaciation, especially for the ice sheets of Greenland and Antarctica where polythermal and cold-based glaciers are warming and sliding may increase (e.g., Moon et al., 2012; Mougnot et al., 2014; Overeem et al., 2017).

4.4 Age of the glacial landscape

In many places throughout the Alps, significant modelled cumulative erosion occurs far inside the Alpine valleys (Fig. 1). However, the potential erosion patterns experience spatial shifts through the glacial cycle (Fig. 3), so that high-altitude rapid
 215 erosion is not modelled to date from expansive glaciation stages, but instead from stages of intermediate glacier cover (Fig. 4; Barr et al., 2019).

For instance, low-elevation piedmont over-deepened basins such as Lake Constance (Fig. 8a), Lake Geneva and Lake Maggiore are here modelled to be the product of extensive Last Glacial Maximum-like glaciations. Other modelling work suggests that features such as these likely form when water can access the glacier bed and encourage glacier sliding and, thus, erosion
 220 (Herman et al., 2011). The model herein does not include subglacial hydrology, yet the role of climate warming to increasing glacier erosion to the lower elevations remains evident (Fig. 4). Alpine terrain with elevations above 1000 m are modelled to experience virtually no erosion from 35 to 18 ka BP (Fig. 4), so that many of the most spectacular, intermediate-elevation glacial valleys of the Alps as Lauterbrunnental, Haslital (Upper Aare) or Bout du Monde (Upper Giffre, Fig. 8b) would date from periods of intermediate glacier extension.

225 The validity of the model results at high elevation is discussable. Crystalline massifs such as the Ecrins, Gran Paradiso, Monte Rosa, Aare, Ötztal and Tauern Massifs locally exhibit a strikingly high erosion potential. However, the computation of glacier flow velocities on such steep surfaces is strongly limited by the model horizontal resolution of 1 km, the shallow-ice

glacier flow physics (Imhof et al., 2019), and PISM's current mass-conservation heuristics (Imhof, 2021, appendix). Besides, bergschrund (rimaye) processes likely to dominate interglacial cirque erosion at such altitudes (Sanders et al., 2012) are not captured by the velocity-based glacier erosion power-laws. Nevertheless, the lack of rapid erosion at high elevations for much of the modelled glacial cycle (Fig. 4) implies that the highest mountain cirques (e.g. Fig. 8c) would have formed over interglacial periods, when glaciers are confined to high terrain (Barr et al., 2017, 2019). Similar processes also occur on Himalayan glaciers and may limit erosion for the high elevation portion of that mountain range during cold periods as well, failing to offset uplift rates (Harper and Humphrey, 2003). Over longer timescales, though, the vertical distribution of erosion rates also depends on the erosional modification of topography (Sternai et al., 2013).

Finally, the time-transgressive nature of the modelled glacial erosion rates hint at a new explanation for the Alpine glacier trim-line and lack of cold-based glaciation evidence. Due to their geographic location in the mid-latitudes, and their steep topographic gradient, the Alps appear as a mountain range that hosted glaciers of various sizes throughout the varying climate of the Quaternary, resulting in a transgressive localization of glacier erosion throughout their elevational range, from the piedmont during glacial maxima, to the highest cirques during interglacial periods. The Alpine trim-line, in this case, would neither correspond to the upper reach of the Last Glacial Maximum glaciers (e.g., Kelly et al., 2004), nor to an englacial temperate-ice boundary (Coutterand, 2010; Seguinot et al., 2018), but to a time-transgressive upper limit of erosion from advancing and retreating glaciers on steep terrain.

5 Conclusions

Due to compounded uncertainties regarding paleoclimate, glacier sliding and erosion processes, our quantitative results are very likely inaccurate. However, we draw the following qualitative conclusions:

- The non-linear physics of glacier deformation and sliding, combined with non-linear empirical erosion laws, results in a very strong localization of rapid glacier erosion in regions of fast flow.
- This high spatio-temporal variability hints at a complex relationship between climate and glacier erosion, so that a highly variable response of glacier erosion to climate should be expected.
- Increased gravitational drag due to surface profile steepening provides a mechanism for accelerated erosion during deglaciation periods, irrespective of surface meltwater penetration to the glacier bed.
- If a non-linear glacier erosion law is used, the climate-induced slowdown of erosion counterbalances glacier expansion, so that Alpine-wide glacier erosion volumes do not correlate with the ice volume.
- Rapid glacier erosion is restricted to low elevation during stages of glacier advance and maximum glaciation, but propagates up-valley to higher elevations during periods of glacier retreat.
- The diversity of the Alpine glacier erosion landscape appears to be the time-transgressive signature of a variety of glacial stages ranging from pan-Alpine ice sheets to modern-style mountain glaciers.

Code and data availability. PISM is available as open-source software (<http://pism-docs.org>). Time and domain-aggregated erosion variables such as used in the figures is available for the four presented erosion power-laws (<https://doi.org/10.5281/zenodo.4495419>). Other model output variables were previously made available (<https://doi.org/10.5281/zenodo.3604174>, <https://doi.org/10.5281/zenodo.3604142>).

Video supplement. Animations made available online show the spatio-temporal distribution of modelled glacier potential erosion rates (<https://vimeo.com/503162771>, supplementing Fig. 1), the evolving relationship between ice volume and potential annual erosion volume (<https://vimeo.com/512478926>, supplementing Fig. 2), and the distribution of potential erosion rate against bedrock altitude (<https://vimeo.com/512479008>, supplementing Fig. 4).

Author contributions. J. Seguinot performed the computations and prepared the figures. I. Delaney interpreted the results in a broader context. Both authors contributed to the text.

Competing interests. The authors declare that they have no conflict of interest.

Acknowledgements. We are very thankful to Constantine Khroulev, Ed Bueler, and Andy Aschwanden for their constant help and development with PISM, without whom this work would not have been possible. J. Seguinot would like to thank John Jansen and Martin Margold for insightful early discussions, Susan Ivy-Ochs for being a constant (droid) motivator, Popi, Mattheos, Karsta, Stefan, Françoise and Dominique for welcoming him on Anafi and providing agreeable conditions for work in times of pandemic, and the Long Haul Trucker for conveying his laptop and data unbroken for 5000 km across Europe and fourteen countries. I. Delaney thanks Frédéric Herman for valuable support and conversations while at University of Lausanne. Both authors thank an anonymous reviewer and Ian Evans (aided by Iestyn Barr, Jeremy Ely, Matt Tomkins, Pippa Whitehouse, Cristina Balaban and Matt Wiecek) for providing constructive feedback which has been incorporated in the present paper, and the associate editor Andreas Lang for handling the reviews. The (previously published) ice flow simulations were made with computer resources provided by the Swiss National Supercomputing Centre (CSCS) allocations no. s573 and sm13 to J. Seguinot.

References

- Albrecht, T., Winkelmann, R., and Levermann, A.: Glacial-cycle simulations of the Antarctic Ice Sheet with the Parallel Ice Sheet Model (PISM) – Part 1: Boundary conditions and climatic forcing, *The Cryosphere*, 14, 599–632, <https://doi.org/10.5194/tc-14-599-2020>, 2020a.
- Albrecht, T., Winkelmann, R., and Levermann, A.: Glacial-cycle simulations of the Antarctic Ice Sheet with the Parallel Ice Sheet Model (PISM) – Part 2: Parameter ensemble analysis, *The Cryosphere*, 14, 633–656, <https://doi.org/10.5194/tc-14-633-2020>, 2020b.
- Alley, R. B., Cuffey, K. M., Evenson, E. B., Strasser, J. C., Lawson, D. E., and Larson, G. J.: How glaciers entrain and transport basal sediment: physical constraints, *Quaternary Sci. Rev.*, 16, 1017–1038, [https://doi.org/10.1016/S0277-3791\(97\)00034-6](https://doi.org/10.1016/S0277-3791(97)00034-6), 1997.
- Alley, R. B., Cuffey, K. M., and Zoet, L. K.: Glacial erosion: status and outlook, *Ann. Glaciol.*, 60, 1–13, <https://doi.org/10.1017/aog.2019.38>, 2019.
- Anderson, L. and Anderson, R.: Modeling debris-covered glaciers: response to steady debris deposition, *The Cryosphere*, 10, 1105, <https://doi.org/10.5194/tc-10-1105-2016>, 2016.
- Anderson, R., Dühnforth, M., Colgan, W., and Anderson, L.: Far-flung moraines: Exploring the feedback of glacial erosion on the evolution of glacier length, *Geomorphology*, 179, 269–285, <https://doi.org/10.1016/j.geomorph.2012.08.018>, 2012.
- Barr, I., Ely, J., Spagnolo, M., Clark, C., Evans, I., Pellicer, X., Pellitero, R., and Rea, B.: Climate patterns during former periods of mountain glaciation in Britain and Ireland: Inferences from the cirque record, *Palaeogeogr., Palaeoclimatol., Palaeoecol.*, 485, 466 – 475, <https://doi.org/10.1016/j.palaeo.2017.07.001>, 2017.
- Barr, I., Ely, J., Spagnolo, M., Evans, I., and Tomkins, M.: The dynamics of mountain erosion: cirque growth slows as landscapes age, *Earth Surf. Processes and Landforms*, 44, 2628–2637, <https://doi.org/10.1002/esp.4688>, 2019.
- Beaud, F., Flowers, G. E., and Pimentel, S.: Seasonal-scale abrasion and quarrying patterns from a two-dimensional ice-flow model coupled to distributed and channelized subglacial drainage, *Geomorphology*, 219, 176–191, <https://doi.org/10.1016/j.geomorph.2014.04.036>, 2014.
- Beaud, F., Venditti, J., Flowers, G., and Koppes, M.: Excavation of subglacial bedrock channels by seasonal meltwater flow, *Earth Surf. Processes and Landforms*, 43, 1960–1972, <https://doi.org/10.1002/esp.4367>, 2018.
- Bendixen, M., Iversen, L. L., Bjørk, A. A., Elberling, B., Westergaard-Nielsen, A., Overeem, I., Barnhart, K. R., Khan, S. A., Abermann, J., Langley, K., et al.: Delta progradation in Greenland driven by increasing glacial mass loss, *Nature*, 550, 101, <https://doi.org/10.1038/nature23873>, 2017.
- Cook, S. J., Swift, D. A., Kirkbride, M. P., Knight, P. G., and Waller, R. I.: The empirical basis for modelling glacial erosion rates, *Nature Communications*, 11, <https://doi.org/10.1038/s41467-020-14583-8>, 2020.
- Coutterand, S.: Etude géomorphologique des flux glaciaires dans les Alpes nord-occidentales au Pléistocène récent : du maximum de la dernière glaciation aux premières étapes de la déglaciation, Ph.D. thesis, Université de Savoie, 2010.
- Dansgaard, W., Johnsen, S. J., Clausen, H. B., Dahl-Jensen, D., Gundestrup, N. S., Hammer, C. U., Hvidberg, C. S., Steffensen, J. P., Sveinbjörnsdóttir, A. E., Jouzel, J., and Bond, G.: Evidence for general instability of past climate from a 250-kyr ice-core record, *Nature*, 364, 218–220, <https://doi.org/10.1038/364218a0>, data archived at the World Data Center for Paleoclimatology, Boulder, Colorado, USA., 1993.
- Dee, D. P., Uppala, S. M., Simmons, A. J., Berrisford, P., Poli, P., Kobayashi, S., Andrae, U., Balmaseda, M. A., Balsamo, G., Bauer, P., Bechtold, P., Beljaars, A. C. M., van de Berg, L., Bidlot, J., Bormann, N., Delsol, C., Dragani, R., Fuentes, M., Geer, A. J., Haimberger, L., Healy, S. B., Hersbach, H., Hólm, E. V., Isaksen, L., Kållberg, P., Köhler, M., Matricardi, M., McNally, A. P., Monge-Sanz, B. M., Mor-

- 315 crette, J.-J., Park, B.-K., Peubey, C., de Rosnay, P., Tavolato, C., Thépaut, J.-N., and Vitart, F.: The ERA-Interim reanalysis: configuration and performance of the data assimilation system, *Q. J. Roy. Meteor. Soc.*, 137, 553–597, <https://doi.org/10.1002/qj.828>, 2011.
- Delaney, I. and Adhikari, S.: Increased subglacial sediment discharge during century scale glacier retreat: consideration of ice dynamics, glacial erosion and fluvial sediment transport, *Geophys. Res. Lett.*, p. e2019GL085672, <https://doi.org/10.1029/2019GL085672>, 2020.
- Delaney, I., Werder, M. A., and Farinotti, D.: A numerical model for fluvial transport of subglacial sediment, *J. Geophys. Res. Earth Surf.*, 124, 2197–2223, <https://doi.org/10.1029/2019jf005004>, 2019.
- 320 Egholm, D., Nielsen, S., Pedersen, V., and Lesemann, J.-E.: Glacial effects limiting mountain height, *Nature*, 460, 884–887, <https://doi.org/10.1038/nature08263>, 2009.
- Egholm, D., Pedersen, V., Knudsen, M., and Larsen, N.: Coupling the flow of ice, water, and sediment in a glacial landscape evolution model, *Geomorphology*, 141–142, 47–66, <https://doi.org/10.1016/j.geomorph.2011.12.019>, 2012a.
- Egholm, D., Pedersen, V., Knudsen, M., and Larsen, N.: On the importance of higher order ice dynamics for glacial landscape evolution, *Geomorphology*, 141–142, 67–80, <https://doi.org/10.1016/j.geomorph.2011.12.020>, 2012b.
- 325 Ehlers, J., Gibbard, P. L., and Hughes, P. D., eds.: vol. 15 of *Dev. Quaternary Sci.*, Elsevier, Amsterdam, 2011.
- Fabel, D., Ballantyne, C. K., and Xu, S.: Trimlines, blockfields, mountain-top erratics and the vertical dimensions of the last British-Irish Ice Sheet in NW Scotland, *Quaternary Sci. Rev.*, 55, 91–102, <https://doi.org/10.1016/j.quascirev.2012.09.002>, 2012.
- Fernandez, R., Anderson, J., Wellner, J., Minzoni, R., Hallet, B., and Smith, R. T.: Latitudinal variation in glacial erosion rates from Patagonia and the Antarctic Peninsula (46 S–65 S), *B. Geol. Soc. Am.*, 128, 1000–1023, <https://doi.org/10.1130/B31321.1>, 2016.
- 330 Fu, P., Heyman, J., Hättstrand, C., Stroeven, A. P., and Harbor, J. M.: Glacial geomorphology of the Shaluli Shan area, southeastern Tibetan Plateau, *J. Maps*, 8, 48–55, <https://doi.org/10.1080/17445647.2012.668762>, 2012.
- Fu, P., Harbor, J. M., Stroeven, A. P., Hättstrand, C., Heyman, J., and Zhou, L.: Glacial geomorphology and paleoglaciation patterns in Shaluli Shan, the southeastern Tibetan Plateau — Evidence for polythermal ice cap glaciation, *Geomorphology*, 182, 66–78, <https://doi.org/10.1016/j.geomorph.2012.10.030>, 2013.
- 335 Ganti, V., von Hagke, C., Scherler, D., Lamb, M., Fischer, W., and Avouac, J.-P.: Time scale bias in erosion rates of glaciated landscapes, *Science Advances*, 2, <https://doi.org/10.1126/sciadv.1600204>, 2016.
- Hallet, B.: A theoretical model of glacial abrasion, *J. Glaciol.*, 23, 39–50, <https://doi.org/10.3189/s0022143000029725>, 1979.
- Hallet, B.: Glacial quarrying: a simple theoretical model, *Ann. Glaciol.*, 22, 1–8, <https://doi.org/10.3189/1996aog22-1-1-8>, 1996.
- 340 Harbor, J. M., Hallet, B., and Raymond, C. F.: A numerical model of landform development by glacial erosion, *Nature*, 333, 347–349, <https://doi.org/10.1038/333347a0>, 1988.
- Harper, J. and Humphrey, N.: High altitude Himalayan climate inferred from glacial ice flux, *Geophys. Res. Lett.*, 30, <https://doi.org/https://doi.org/10.1029/2003GL017329>, 2003.
- Herman, F. and Champagnac, J.-D.: Plio-Pleistocene increase of erosion rates in mountain belts in response to climate change, *Terra Nova*, 28, 2–10, <https://doi.org/10.1111/ter.12186>, 2016.
- 345 Herman, F., Beaud, F., Champagnac, J., Lemieux, J. M., and Sternai, P.: Glacial hydrology and erosion patterns: a mechanism for carving glacial valleys, *Earth Planet. Sc. Lett.*, 310, 498–508, <https://doi.org/10.1016/j.epsl.2011.08.022>, 2011.
- Herman, F., Beysac, O., Brughelli, M., Lane, S. N., Leprince, S., Adatte, T., Lin, J. Y. Y., Avouac, J.-P., and Cox, S. C.: Erosion by an Alpine glacier, *Science*, 350, 193–195, <https://doi.org/10.1126/science.aab2386>, 2015.
- 350 Hewitt, I. and Creyts, T.: A model for the formation of eskers, *Geophys. Res. Lett.*, 46, 6673–6680, <https://doi.org/10.1029/2019GL082304>, 2019.

- Hijmans, R. J., Cameron, S. E., Parra, J. L., Jones, P. G., and Jarvis, A.: Very high resolution interpolated climate surfaces for global land areas, *Int. J. Climatol.*, 25, 1965–1978, <https://doi.org/10.1002/joc.1276>, 2005.
- Hildes, D. H., Clarke, G. K., Flowers, G. E., and Marshall, S. J.: Subglacial erosion and englacial sediment transport modelled for North American ice sheets, *Quaternary Sci. Rev.*, 23, 409–430, <https://doi.org/10.1016/j.quascirev.2003.06.005>, 2004.
- Humphrey, N. F. and Raymond, C. F.: Hydrology, erosion and sediment production in a surging glacier: Variegated Glacier, Alaska, 1982–83, *J. Glaciol.*, 40, 539–552, <https://doi.org/10.3189/s0022143000012429>, 1994.
- Huss, M., Jouvét, G., Farinotti, D., and Bauder, A.: Future high-mountain hydrology: a new parameterization of glacier retreat, *Hydrol. Earth Syst. Sc.*, 14, 815–829, <https://doi.org/10.5194/hess-14-815-2010>, 2010.
- Huybrechts, P.: Sea-level changes at the LGM from ice-dynamic reconstructions of the Greenland and Antarctic ice sheets during the glacial cycles, *Quaternary Sci. Rev.*, 21, 203–231, [https://doi.org/10.1016/s0277-3791\(01\)00082-8](https://doi.org/10.1016/s0277-3791(01)00082-8), 2002.
- Imhof, M.: Combined climate-ice flow modelling of the Alpine ice field during the Last Glacial Maximum, Ph.D. thesis, ETH Zürich, <https://doi.org/10.3929/ethz-b-000471073>, 2021.
- Imhof, M. A., Cohen, D., Seguinot, J., Aschwanden, A., Funk, M., and Jouvét, G.: Modelling a paleo valley glacier network using a hybrid model: an assessment with a Stokes ice flow model, *J. Glaciol.*, 65, 1000–1010, <https://doi.org/10.1017/jog.2019.77>, 2019.
- Iverson, N. R.: A theory of glacial quarrying for landscape evolution models, *Geology*, 40, 679–682, <https://doi.org/10.1130/G33079.1>, 2012.
- Jansen, J., Knudsen, M., Andersen, J., Heyman, J., and Egholm, D.: Erosion rates in Fennoscandia during the past million years, *Quaternary Sci. Rev.*, 207, 37–48, <https://doi.org/10.1016/j.quascirev.2019.01.010>, 2019.
- Jarvis, A., Reuter, H., Nelson, A., and Guevara, E.: Hole-filled SRTM for the globe Version 4, available from the CGIAR-CSI SRTM 90m Database, <http://srtm.csi.cgiar.org>, 2008.
- Jouzel, J., Masson-Delmotte, V., Cattani, O., Dreyfus, G., Falourd, S., Hoffmann, G., Minster, B., Nouet, J., Barnola, J. M., Chappellaz, J., Fischer, H., Gallet, J. C., Johnsen, S., Leuenberger, M., Loulergue, L., Luethi, D., Oerter, H., Parrenin, F., Raisbeck, G., Raynaud, D., Schilt, A., Schwander, J., Selmo, E., Souchez, R., Spahni, R., Stauffer, B., Steffensen, J. P., Stenni, B., Stocker, T. F., Tison, J. L., Werner, M., and Wolff, E. W.: Orbital and Millennial Antarctic Climate Variability over the Past 800,000 Years, *Science*, 317, 793–796, <https://doi.org/10.1126/science.1141038>, data archived at the World Data Center for Paleoclimatology, Boulder, Colorado, USA., 2007.
- Kelly, M. A., Buoncristiani, J.-F., and Schlüchter, C.: A reconstruction of the last glacial maximum (LGM) ice surface geometry in the western Swiss Alps and contiguous Alpine regions in Italy and France, *Eclogae geol. Helv.*, pp. 57–75, <https://doi.org/10.1007/s00015-004-1109-6>, 2004.
- Kleman, J.: Preservation of landforms under ice sheets and ice caps, *Geomorphology*, 9, 19–32, [https://doi.org/10.1016/0169-555x\(94\)90028-0](https://doi.org/10.1016/0169-555x(94)90028-0), 1994.
- Kleman, J., Stroeven, A. P., and Lundqvist, J.: Patterns of Quaternary ice sheet erosion and deposition in Fennoscandia and a theoretical framework for explanation, *Geomorphology*, 97, 73–90, <https://doi.org/10.1016/j.geomorph.2007.02.049>, 2008.
- Kleman, J., Jansson, K., De Angelis, H., Stroeven, A., Hättestrand, C., Alm, G., and Glasser, N.: North American ice sheet build-up during the last glacial cycle, 115–21 kyr, *Quaternary Sci. Rev.*, 29, 2036–2051, <https://doi.org/10.1016/j.quascirev.2010.04.021>, 2010.
- Koppes, M., Hallet, B., Rignot, E., Mouginit, J., Wellner, J. S., and Boldt, K.: Observed latitudinal variations in erosion as a function of glacier dynamics, *Nature*, 526, 100–103, <https://doi.org/10.1038/nature15385>, 2015.
- Koppes, M. N. and Montgomery, D. R.: The relative efficacy of fluvial and glacial erosion over modern to orogenic timescales, *Nature Geoscience*, 2, 644–647, <https://doi.org/10.1038/ngeo616>, 2009.

- Lai, J. and Anders, A. M.: Climatic controls on mountain glacier basal thermal regimes dictate spatial patterns of glacial erosion, *Earth Surf. Dynam. Discuss.* [preprint], <https://doi.org/10.5194/esurf-2021-26>, in review, 2021.
- 390 Lane, S. N., Bakker, M., Gabbud, C., Micheletti, N., and Saugy, J.: Sediment export, transient landscape response and catchment-scale connectivity following rapid climate warming and alpine glacier recession, *Geomorphology*, 277, 210 – 227, <https://doi.org/10.1016/j.geomorph.2016.02.015>, 2017.
- Lisiecki, L. E. and Raymo, M. E.: A Pliocene-Pleistocene stack of 57 globally distributed benthic $\delta^{18}\text{O}$ records, *Paleoceanography*, 20, PA1003, <https://doi.org/10.1029/2004pa001071>, 2005.
- 395 MacGregor, K., Anderson, R., Anderson, S., and Waddington, E.: Numerical simulations of glacial-valley longitudinal profile evolution, *Geology*, 28, 1031–1034, [https://doi.org/10.1130/0091-7613\(2000\)28<1031:NSOGLP>2.0.CO;2](https://doi.org/10.1130/0091-7613(2000)28<1031:NSOGLP>2.0.CO;2), 2000.
- Margold, M., Jansson, K. N., Kleman, J., and Stroeven, A. P.: Glacial meltwater landforms of central British Columbia, *J. Maps*, 7, 486–506, <https://doi.org/10.4113/jom.2011.1205>, 2011.
- 400 Mariotti, A., Blard, P.-H., Charreau, J., Toucanne, S., Jorry, S., Molliex, S., Bourlès, D., Aumaitre, G., and Keddadouche, K.: Nonlinear forcing of climate on mountain denudation during glaciations, *Nature Geoscience*, pp. 1–7, <https://doi.org/10.1038/s41561-020-00672-2>, 2021.
- Martrat, B., Grimalt, J. O., Shackleton, N. J., de Abreu, L., Hutterli, M. A., and Stocker, T. F.: Four climate cycles of recurring deep and surface water destabilizations on the Iberian margin, *Science*, 317, 502–507, <https://doi.org/10.1126/science.1139994>, 2007.
- 405 Micheletti, N. and Lane, S. N.: Water yield and sediment export in small, partially glaciated Alpine watersheds in a warming climate, *Water Resources Res.*, 52, 4924–4943, <https://doi.org/10.1002/2016WR018774>, 2016.
- Moon, T., Joughin, I., Smith, B., and Howat, I.: 21st-Century Evolution of Greenland Outlet Glacier Velocities, *Science*, 336, 576–578, <https://doi.org/10.1126/science.1219985>, 2012.
- Mouginot, J., Rignot, E., and Scheuchl, B.: Sustained increase in ice discharge from the Amundsen Sea Embayment, West Antarctica, from 1973 to 2013, *Geophys. Res. Lett.*, 41, 1576–1584, <https://doi.org/https://doi.org/10.1002/2013GL059069>, 2014.
- 410 Overeem, I., Hudson, B. D., Syvitski, J. P. M., Mikkelsen, A. B., Hasholt, B., van den Broeke, M. R., Noël, B. P. Y., and Morlighem, M.: Substantial export of suspended sediment to the global oceans from glacial erosion in Greenland, *Nature Geoscience*, 10, 859–863, <https://doi.org/10.1038/NGEO3046>, 2017.
- Patterson, T. and Kelso, N. V.: Natural Earth. Free vector and raster map data, <http://naturalearthdata.com>, 2017.
- 415 Pedersen, V. K., Huisman, R. S., Herman, F., and Egholm, D. L.: Controls of initial topography on temporal and spatial patterns of glacial erosion, *Geomorphology*, 223, 96–116, <https://doi.org/10.1016/j.geomorph.2014.06.028>, 2014.
- Penck, A.: Glacial Features in the Surface of the Alps, *J. Geol.*, 13, 1–19, <https://doi.org/10.1086/621202>, 1905.
- Preusser, F., Reitner, J. M., and Schlüchter, C.: Distribution, geometry, age and origin of overdeepened valleys and basins in the Alps and their foreland, *Swiss J. Geosci.*, 103, 407–426, 2010.
- 420 Preusser, F., Graf, H. R., Keller, O., Krayss, E., and Schlüchter, C.: Quaternary glaciation history of northern Switzerland, *Quaternary Sci. J.*, 60, 282–305, <https://doi.org/10.3285/eg.60.2-3.06>, 2011.
- Sanders, J. W., Cuffey, K. M., Moore, J. R., MacGregor, K. R., and Kavanaugh, J. L.: Periglacial weathering and headwall erosion in cirque glacier bergschrunds, *Geology*, 40, 779–782, <https://doi.org/10.1130/g33330.1>, 2012.
- Seguinot, J.: Glacial quarrying and development of overdeepenings in glacial valleys: modelling experiments and case studies at Erdalen, Western Norway, <https://doi.org/10.31237/osf.io/8fzd6>, 2008.
- 425

- Seguinot, J.: Numerical modelling of the Cordilleran ice sheet, Ph.D. thesis, Stockholm University, <http://urn.kb.se/resolve?urn=urn:nbn:se:su:diva-106815>, 2014.
- Seguinot, J.: Alpine ice sheet glacial cycle simulations aggregated variables [data set], Zenodo, <https://doi.org/10.5281/zenodo.3604174>, 2020a.
- 430 Seguinot, J.: Alpine ice sheet glacial cycle simulations continuous variables [data set], Zenodo, <https://doi.org/10.5281/zenodo.3604142>, 2020b.
- Seguinot, J.: Alpine ice sheet erosion potential aggregated variables [data set], Zenodo, <https://doi.org/10.5281/zenodo.4495419>, 2021.
- Seguinot, J., Rogozhina, I., Stroeven, A. P., Margold, M., and Kleman, J.: Numerical simulations of the Cordilleran ice sheet through the last glacial cycle, *The Cryosphere*, 10, 639–664, <https://doi.org/10.5194/tc-10-639-2016>, 2016.
- 435 Seguinot, J., Ivy-Ochs, S., Jouvet, G., Huss, M., Funk, M., and Preusser, F.: Modelling last glacial cycle ice dynamics in the Alps, *The Cryosphere*, 12, 3265–3285, <https://doi.org/10.5194/tc-12-3265-2018>, 2018.
- Steinemann, O., Ivy-Ochs, S., Grazioli, S., Luetscher, M., Fischer, U. H., Vockenhuber, C., and Synal, H.-A.: Quantifying glacial erosion on a limestone bed and the relevance for landscape development in the Alps, *Earth Surf. Processes and Landforms*, 45, 1401–1417, <https://doi.org/10.1002/esp.4812>, 2020.
- 440 Steinemann, O., Ivy-Ochs, S., Hippe, K., Christl, M., Haghpor, N., and Synal, H.-A.: Glacial erosion by the Trift glacier (Switzerland): Deciphering the development of riegels, rock basins and gorges, *Geomorphology*, 375, 107 533, <https://doi.org/10.1016/j.geomorph.2020.107533>, 2021.
- Sternai, P., Herman, F., Valla, P. G., and Champagnac, J.-D.: Spatial and temporal variations of glacial erosion in the Rhone valley (Swiss Alps): Insights from numerical modeling, *Earth Planet. Sc. Lett.*, 368, 119 – 131, 2013.
- 445 the PISM authors: PISM, a Parallel Ice Sheet Model, <http://www.pism-docs.org>, 2017.
- Thomson, S., Brandon, M., Tomkin, J., Reiners, P., Vásquez, C., and Wilson, N.: Glaciation as a destructive and constructive control on mountain building, *Nature*, 467, 313–317, <https://doi.org/10.1038/nature09365>, 2010.
- Tulaczyk, S., Kamb, W. B., and Engelhardt, H. F.: Basal mechanics of Ice Stream B, west Antarctica: 1. Till mechanics, *J. Geophys. Res.*, 105, 463, <https://doi.org/10.1029/1999jb900329>, 2000.
- 450 Ugelvig, S., Egholm, D., Anderson, R., and Iverson, N.: Glacial erosion driven by variations in meltwater drainage, *J. Geophys. Res. Earth Surf.*, 123, <https://doi.org/10.1029/2018JF004680>, 2018.
- Valla, P. G., Shuster, D. L., and van der Beek, P. A.: Significant increase in relief of the European Alps during mid-Pleistocene glaciations, *Nature Geoscience*, 4, 688–692, <https://doi.org/10.1038/ngeo1242>, 2011.
- Werder, M. A., Hewitt, I. J., Schoof, C. G., and Flowers, G. E.: Modeling channelized and distributed subglacial drainage in two dimensions, *J. Geophys. Res. Earth Surf.*, 118, 2140–2158, <https://doi.org/10.1002/jgrf.20146>, 2013.
- 455 Willenbring, J. and Von Blanckenburg, F.: Long-term stability of global erosion rates and weathering during late-Cenozoic cooling, *Nature*, 465, 211–214, <https://doi.org/10.1038/nature09044>, 2010.
- Wirsig, C., Zasadni, J., Christl, M., Akçar, N., and Ivy-Ochs, S.: Dating the onset of LGM ice surface lowering in the High Alps, *Quaternary Sci. Rev.*, 143, 37–50, <https://doi.org/10.1016/j.quascirev.2016.05.001>, 2016.
- 460 Zekollari, H. and Huybrechts, P.: On the climate–geometry imbalance, response time and volume–area scaling of an alpine glacier: insights from a 3-D flow model applied to Vadret da Morteratsch, Switzerland, *Ann. Glaciol.*, 56, 51–62, <https://doi.org/10.3189/2015aog70a921>, 2015.